Finite Difference Modeling of Seismic Responses to Intersecting Fracture Sets

Shihong Chi, Yang Zhang, Xander Campman and M. Nafi Toksöz
Earth Resources Laboratory
Dept. of Earth, Atmospheric, and Planetary Sciences
Massachusetts Institute of Technology
Cambridge, MA 02139

May 27, 2006

Abstract

Fractured reservoir characterization is becoming increasingly important for the petroleum industry. Current methods for this task are developed based on effective media theory, which assumes the cracks or fractures in a reservoir are much smaller than the seismic wavelength. A discrete fracture model has to be used for large-scale fractures. We describe an approach of using a finite difference method for modeling seismic wave propagation in rock formations with intersecting fracture sets. We then use the code to study the behavior of seismic waves, particularly scattering due to such fracture sets with various spacing and compliances. The scattering pattern due to fractures varies azimuthally. We find that converted PS and PSP waves from the bottom of the fractured layers show strong interference by the scattered waves. We observe coherent scattered waves in shot gathers parallel to the fracture orientation and significant backscattering at near offsets and forward scattering at far offsets in the gathers normal to the fracture orientation. When two sets of fractures are present, scattering becomes stronger and more complex scattered waves appear in the gathers. The scattering becomes stronger with increasing the fracture compliances and decreasing spacing (still on the order of seismic wave length). When the fracture sets are not orthogonal to each other, the gathers still show coherent scattering in the fracture orientations. Azimuthal characteristics of the scattered waves may be used to analyze fracture orientations, spacing, and relative compliance of intersecting fracture sets.

1 Introduction

The purpose of this paper is to describe a finite difference method for modeling seismic wave propagation in rock formations with intersecting fracture sets with spacing on the order of the wavelength or larger. We intend to provide a widely usable tool for aiding developments of methods for extracting orientation, spacing, and compliance of such fracture sets. We study the behavior of seismic waves, particularly scattering due to such fracture sets. Fractured reservoir characterization has drawn increasing attention in the petroleum industry. Many people have studied seismic responses to fractures and characterized fractures using seismic data based on effective media theory, which assumes the fractures are penny shaped cracks (Hudson, 1986; Liu et al., 2000) or the spacing of the fractures sets are much smaller than the seismic wavelength (Schoenberg and Sayers, 1995). Using effective media theory, the fractured rocks can be approximated as homogeneous anisotropic media of lower symmetries. Based on this theory, azimuthal AVO of reflected PP and converted PS waves are commonly used for determining fracture orientation and other parameters

(Vetri et al., 2003; Shen et al., 2002). Schoenberg and Helbig (1997) discussed a geophysically important subset of orthorhombic media consisting of vertically fractured transversely isotropic media with a vertical symmetry axis (VTI) in great detail. They evaluated possible methods to quantify fracture orientation and compliance and background elastic parameters using multi-azimuth surface seismic, VSP and cross-well data. Natural fractures in reservoirs often contain two or more intersecting sets. They can be orthogonal or non-orthogonal depending on the stress history (Reiss, 1980; Nelson, 1985). Nichols et al. (1989) described the problem of modeling rocks with multiple sets of fractures based on the compliance addition theory outlined by Schoenberg and Muir (1989). They also showed explicitly how to obtain the resultant compliance tensor for an orthogonal fracture set embedded in an isotropic medium and that such a fracture set renders the medium orthorhombic. Grechka and Kachanov (2005) studied the effective anisotropy of multiple fractures in rocks, where networks of small fractures control the fluid flow. They concluded that regardless of the number of fracture sets embedded in otherwise isotropic host rock, their orientations, or types of fluid infill, the symmetry of the effective medium is approximately orthorhombic. They also showed that both theories of Schoenberg and Kachanov describe the effective media well. For the long wavelength effect of realistic fractures on seismic responses, i.e., when wavelengths are much larger than the fracture spacing, we use Schoenberg's formulation for the equivalent anisotropic medium in terms of elastic compliance.

The effective media theory has been widely used in various seismic applications.Sayers (1998) analytically determined the misalignment of the orientation of fractures and the principal axes for P and S waves in rocks containing multiple non-orthogonal fracture sets. Schoenberg et al. (1999) showed the azimuth-dependent tuning of seismic waves reflected from a thin reservoir layer containing one or more sets of fractures. Bakulin et al. (2000a,b) and Bakulin et al. (2000c) attempted to invert various seismic signatures for formation parameters.

However, when the fracture spacing is on the order of the seismic wavelength, the effective medium theory cannot capture the effect of fractures. Recent works (Nihei et al., 2002; Lynn, 2004; Willis et al., 2004b,a, 2006) have studied the effect of discrete parallel fractures because geological evidence shows that fractures with spacing on the order of the seismic wavelength commonly exist in reservoirs. Zhang et al. (2005) showed on synthetic seismic data that the azimuthal AVO properties are very different for penny shaped cracks and discrete parallel fractures. In the field, many fractures are not parallel, but intersecting. In modeling seismic responses to small fracture networks and large discrete fractures, it is important to be able to represent the fractures at various scales properly.

Coates and Schoenberg (1995) developed a general formulation for modeling multiple intersecting sets of fractures with arbitrary orientations using a finite difference method. To model a linear-slip fracture when the fracture is at an angle to the finite difference grid, they used a suitable equivalent anisotropic medium to replace the elastic medium within each finite difference cell intersected by the fracture, together with the embedded segment of the fracture. Nihei et al. (2002) and Vlastos et al. (2003) modeled the seismic responses of discrete sets of parallel fractures. We extend their approach to model multiple intersecting sets of fractures. We represent them discretely in our modeling. We present details on how to represent orthogonally and non-orthogonally intersecting fractures in finite difference modeling. We further simplify the model building process, particularly on how to represent the areas near the fracture intersections. Then we study the characteristics of seismic scattering due to intersecting fracture sets.

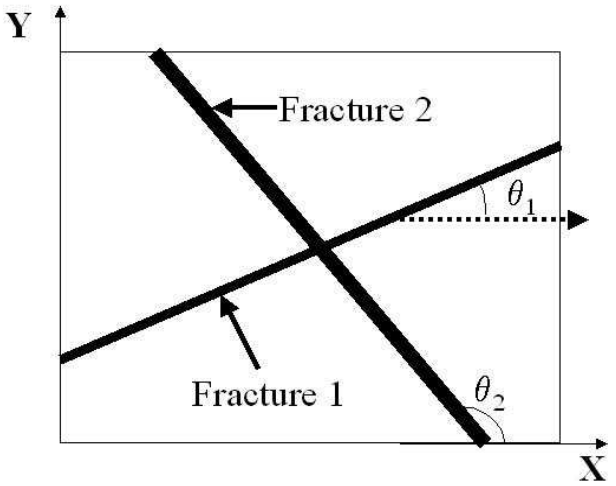

Figure 1: Two intersecting vertical fractures passing through the map view of a 3-D finite-difference cell. Each fracture normal forms an angle θ_i to the finite difference grid direction.

2 Effective Media Theory of Multiple Sets of Fractures

For multiple sets of vertical fractures, Nichols et al. (1989) show that the compliance matrix for the equivalent medium is

$$S = S_b + \sum_{i=q}^{m} \Delta S_i, \tag{1}$$

where m is the number of fracture sets, S_b and ΔS_i are the compliance of background medium and contribution from the i-th fracture set (see Figure 1). It is obvious that the order in which the fractures are included does not affect the final compliance. Assuming the i-th fracture strike forms an angle θ_i to the finite difference grid direction, the Bond transformation matrix can be written as (Auld, 1990)

$$B = \begin{bmatrix} \frac{1+\cos 2\theta_i}{2} & \frac{1+\cos 2\theta_i}{2} & 0 & 0 & 0 & \sin 2\theta_i \\ -\frac{\sin 2\theta_i}{2} & \frac{\sin 2\theta_i}{2} & 0 & 0 & 0 & \cos 2\theta_i \\ 0 & 0 & 0 & \sin 2\theta_i & -\cos\theta_i & 0 \end{bmatrix} \tag{2}$$

and

$$\Delta S_i = B^T Z_i B, \tag{3}$$

where in the fracture coordinate system, the compliance of each fracture set can be written as

$$Z_i = \begin{bmatrix} Z_i^N & 0 & 0 \\ 0 & Z_i^V & 0 \\ 0 & 0 & Z_i^H \end{bmatrix} \tag{4}$$

where Z_i^N, Z_i^V, and Z_i^H represent the normal, vertical and horizontal compliance of the i-th fracture, respectively. A rotationally symmetric fracture has equal vertical and horizontal compliance. Inversion of the compliance matrix yields thpe elastic stiffness matrix. Schoenberg and Sayers (1995) showed that the equivalent media of isotropic host media embedding non-orthogonally and orthogonally intersecting fractures is monoclinic and orthorhombic, respectively. If the formation shows horizontal stratification, we generally represent it as transversely isotropic with a vertical rotation symmetry axis (VTI). If only a set of vertical

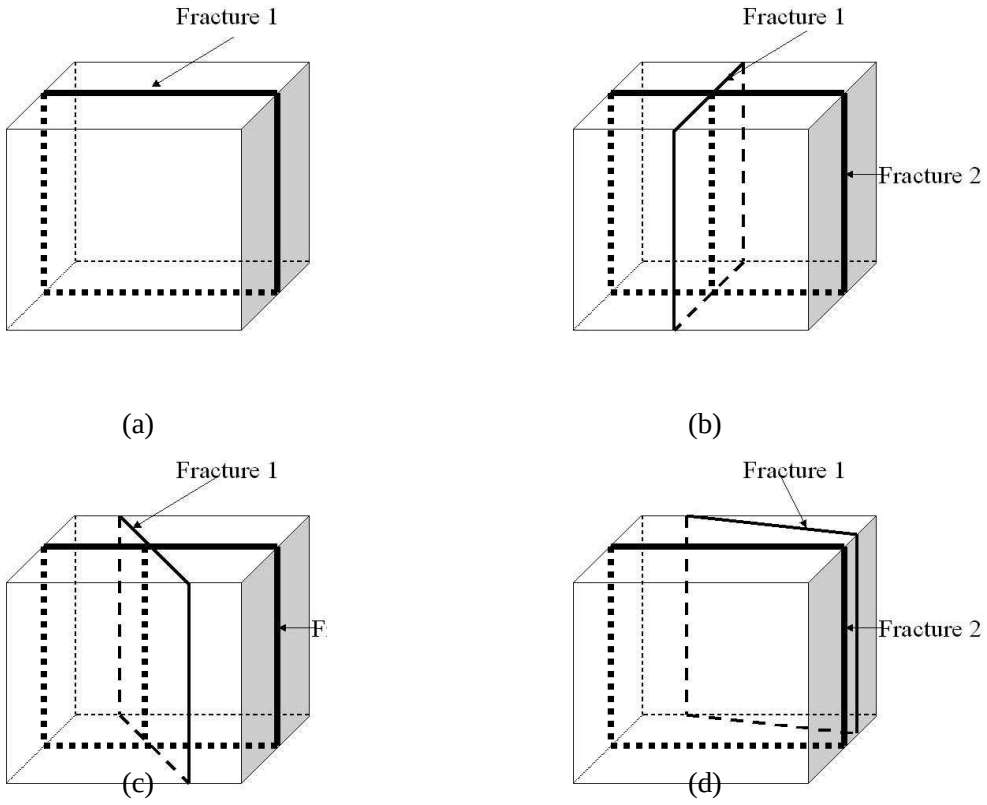

Figure 2: A 3-D finite difference cube containing fracture(s). a. Fracture strike is parallel to one axis; b. Strikes of two orthogonally intersecting fractures are parallel to two axes; c. Only the strike of one of the two orthogonally intersecting fractures is parallel to one axis; d. Only the strike of one of the two non-intersecting fractures is parallel to one axis.

fractures embeds in it, the effective medium property of the fractured formation is orthorhombic (Schoenberg and Helbig, 1997). If two sets of orthogonally intersecting fractures exist in the VTI formation, the effective medium property of the fractured formation should still be orthorhombic. If the two sets are non-orthogonal in the VTI formation, the effective medium property of the fractured formation has been shown to be monoclinic (Winterstein, 1990).

3 Representing Discrete Intersecting Fractures in Finite-Difference Modeling

To model seismic responses due to orthogonally intersecting fracture sets using the finite difference method in a Cartesian coordinate system, we can choose one of the coordinate axes parallel to the fracture strike.

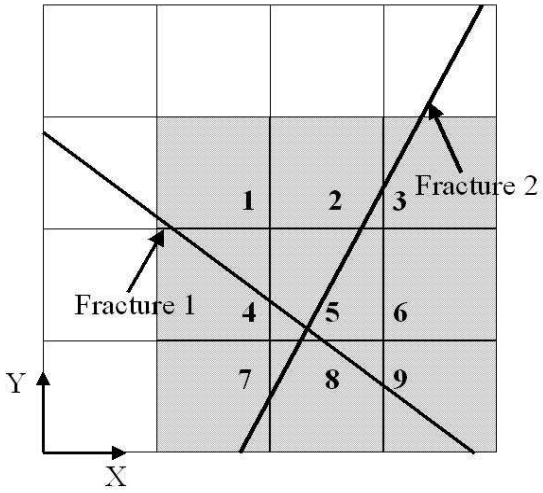

Figure 3: Top view of a set of intersecting fractures overlaying on the finite difference grid. Cells 1 to 9 can use the same property based on effective media theory to reduce the modeling complexity.

We assign the finite difference cells containing only one fracture the equivalent transversely isotropic (with a horizontal rotation symmetry axis) (HTI) elastic property (Figure 2a) and assign the cells containing the intersections the equivalent orthorhombic elastic property (Figure 2b). For non-orthogonally intersecting fracture sets, we can choose one set whose strike will be parallel or normal to the axes (Figure 2c). The finite-difference cells containing intersection(s) of fractures (Figure 2c) possess the properties of monoclinic media (Figure 2d), because the dimension of the grids is much smaller than seismic wavelength and elastic properties of these cells can be approximated using the effective media theory (Schoenberg and Sayers, 1995). For cells containing only fractures normal or parallel to the coordinate axes, we can assign the cell HTI properties. Otherwise, cells only contain the fractures intersecting the axes with an angle other than 0 or 90 degrees. For these cells, we find the elastic stiffness in the current coordinate system using equation 6 and assign them to the respective cells. The properties of these cells show the characteristics of monoclinic media.

To simplify the model building process, we can assign the same parameters to a small region surrounding the intersections based on long wave equivalent media theory. For example, finite difference cells 1 through 9 enclosing the intersection shown in Figure 3 can use the same property if the cell size is much smaller than the seismic wavelength. In some reservoirs, fractures in production zones at different depth show different orientation (Figure 4). In modeling the seismic response using the finite-difference technique, we can choose fractures in one hydrocarbon zone with strike parallel or normal to the axes, while fractures in another zone make an angle with the axes other than 0 or 90 degrees. The apparent elastic stiffness matrix of the other zone resembles that of monoclinic media because of matrix rotation. To simulate the effects of all fractures from the whole field, the finite-difference program has to be able to simulate wave propagation in a monoclinic formation. This situation further shows the need for this study.

4 Finite Difference Implementation

In our finite difference implementation, we use a rotated staggered grid scheme, which allows strong contrasts in the medium and leads to less dispersion errors and a higher computational efficiency (Saenger et al.,

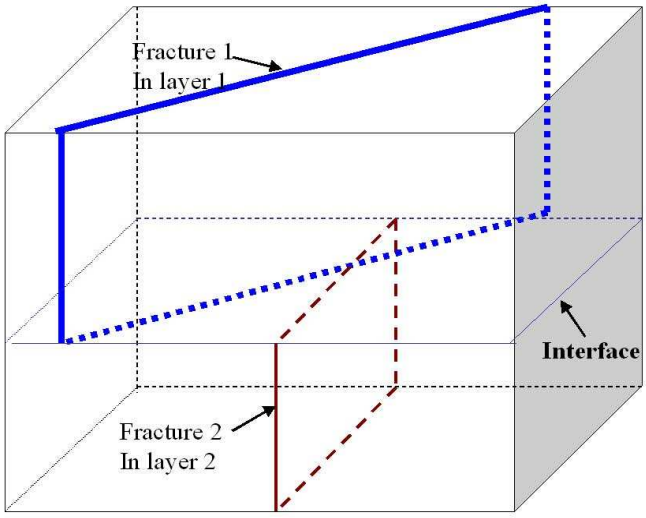

Figure 4: Fractures in different reservoir layers showing different strikes.

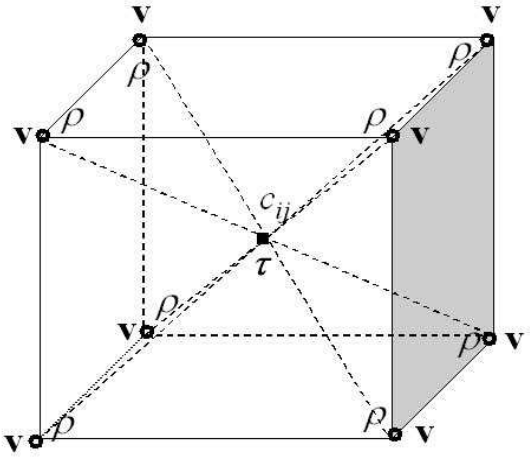

Figure 5: The locations of velocity, stress, and elastic properties in an elementary finite difference cell using rotated staggered grid scheme.

2000). In such a scheme, all components of one physical property (e.g., stress, velocity, elastic stiffness, and density) are placed at one single location as shown in Figure 5. It is not necessary to average any elastic stiffness values as in the standard staggered method (Virieux, 1986). Therefore, this scheme can incorporate the high contrasts existing in fractured media without smoothing the elastic stiffnesses, resulting in a more accurate representation of the fractures.

To effectively absorb wave reflections from the model boundaries, we apply a perfectly matched layer boundary condition (Marcinkovich and Olsen, 2003). We use the first order velocity-stress equations for orthorhombic media. Starting from Hooke's law, we can write:

$$\partial_t \tau_{ij} = \frac{1}{2} c_{ijkl}(v_{k,l} + v_{l,k}). \tag{5}$$

Using the Voigt notation, for orthorombic media, the stiffness tensor c_{ijkl} is given by

$$\boldsymbol{c} = \begin{bmatrix} c_{11} & c_{12} & c_{13} & 0 & 0 & 0 \\ 0 & c_{22} & c_{23} & 0 & 0 & 0 \\ 0 & 0 & c_{33} & 0 & 0 & 0 \\ 0 & 0 & 0 & c_{44} & 0 & 0 \\ 0 & 0 & 0 & 0 & c_{55} & 0 \\ 0 & 0 & 0 & 0 & 0 & c_{66} \end{bmatrix} \tag{6}$$

where τ_{ij} and v_i are elements of the stress tensor and velocity, respectively, and $i, j = x, y, z$. To model wave propagation in non-orthogonal sets of fractures or equivalent monoclinic media, we need to extend equation 6

$$\boldsymbol{c} = \begin{bmatrix} c_{11} & c_{12} & c_{13} & 0 & 0 & c_{16} \\ 0 & c_{22} & c_{23} & 0 & 0 & c_{26} \\ 0 & 0 & c_{33} & 0 & 0 & c_{36} \\ 0 & 0 & 0 & c_{44} & c_{45} & 0 \\ 0 & 0 & 0 & 0 & c_{55} & 0 \\ 0 & 0 & 0 & 0 & 0 & c_{66} \end{bmatrix} \tag{7}$$

Comparing equations 6 and 7, we find that modeling wave propagation in reservoirs containing non-orthogonal fracture systems using the finite difference method demands extra computation cost and memory storage. Otherwise, no additional difficulty occurs.

5 Seismic Scattering due to Intersecting Fractures

In this section, we study the characteristics of the seismic responses from fractured reservoirs. We assume the background formation is isotropic. The fluid filling the fractures is gas. The fractures are 1) orthogonal or 2) non-orthogonal. In both cases, we consider a three-layered model and fractures penetrate through the second layer. Table 1 shows the elastic properties of the background layers. The receiver arrays and the source are located at the earth surface. Figure 6 shows the generic, schematic diagram of the model. In this three-layer reservoir model, the second layer contains the fractures. We first assume the fractures are rotationally invariant and the normal and transverse compliance of the fractures are equal to 2×10^{-10} m/Pa. Therefore, each set of fractures contributes equally to receiver responses. The source and receiver arrays are located at the surface. We use Ricker wavelet as our point source with center frequency at 40 Hz.

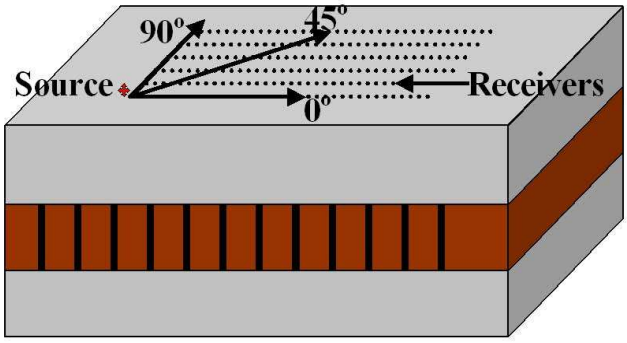

Figure 6: A fractured three-layered reservoir model. Two sets of fractures penetrate through the second layer.

Table 1: The elastic properties of background media for the three-layer model.

	v_p (m/s)	v_s (m/s)	ρ (kg/m^3)	λ_P (m)	λ_S (m)
Top layer	2460	1230	2300	60	30
Middle layer	3300	1800	2200	80	45
Bottom layer	2460	1230	2300	60	30

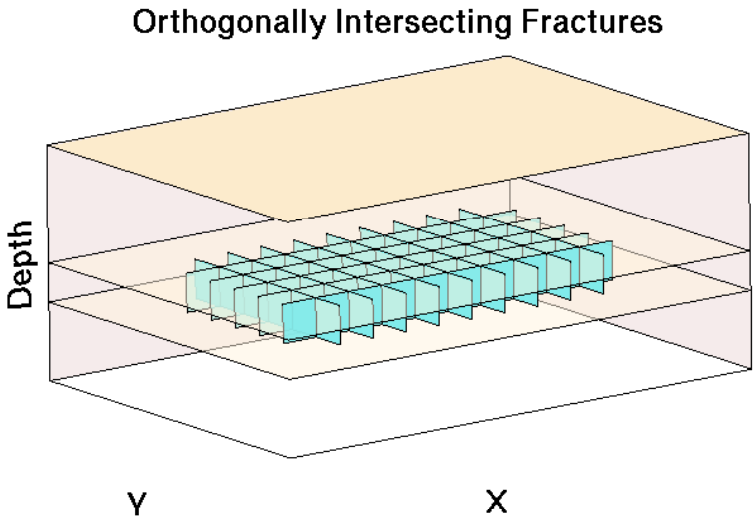

Figure 7: A 3D schematic of the reservoir model with two sets of orthogonally intersecting fractures.

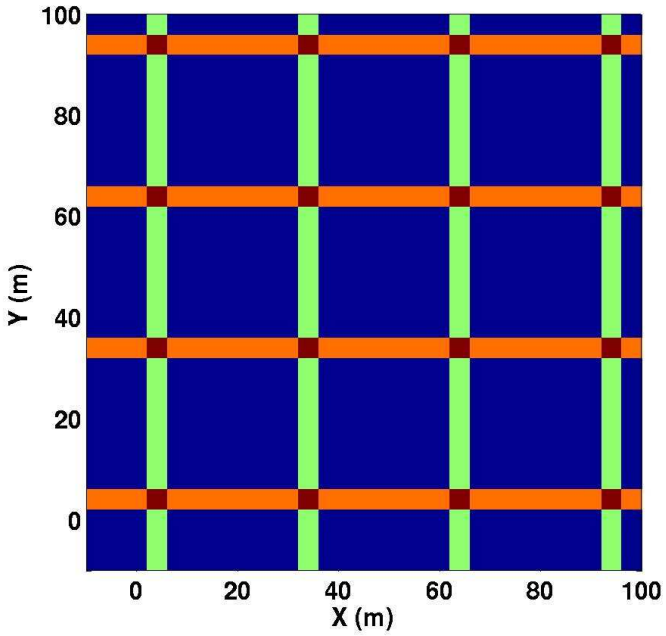

Figure 8: Elastic property distribution of two sets of orthogonally intersecting fractures as indicated by different colors.

5.1 Case 1: Two sets of orthogonally intersecting fractures

We first use the finite difference program to model seismic wave propagation in a medium containing two sets of orthogonally intersecting fractures. Each set of fractures has a regular 30 m spacing. Figure 7 is a 3D schematic of the model. Figure 8 is a zoom-in view of a horizontal slice of the fractured second layer. Different colors represent the background, the two sets of fractures and their intersections.

To understand seismic scattering due to fractures, we also conduct modeling of seismic wave propagation in the same layered background model without fractures and in a model with only one set of parallel vertical fractures of 30 m spacing as references. Figures 9 shows the vertical component of velocity acquired over the 3-layered model without fractures in the middle layer. Figures 10 and 11 show the vertical component of velocity acquired over the model with one set of parallel fracture. Figure 12 and 13 show the vertical component of velocity acquired over the 3-layered model with the orthogonal fractures in the middle layer. In each of the panels, the direct wave has been muted. We have identified reflected and converted waves from the top and bottom of the reservoir.

To identify the events shown in Figure 9, we estimate the arrival times of the P, S, and converted waves from the top and bottom of the middle layer at near offsets. Using these estimated arrival times, we identify the reflected P and P to S waves from the top and bottom of the middle layer. At near offsets, the reflected P wave is very strong and the reflected P to S waves become stronger when the offsets get larger. At intermediate to far offsets, immediately following the reflected P wave from the bottom of the middle layer, a converted PSP wave appears. The shot gathers do not show any azimuthal difference.

Figure 10a shows a line collected over the fractured reservoir perpendicular to the fracture strike. Scattered energy from the fracture zones contaminates the events arriving in later time, especially for PS energy converted at the top and bottom of the reservoir. Strong scattered waves are the dominant energy in this case. Frequency-wavenumber spectra of these data show both forward and backward scattered energy and

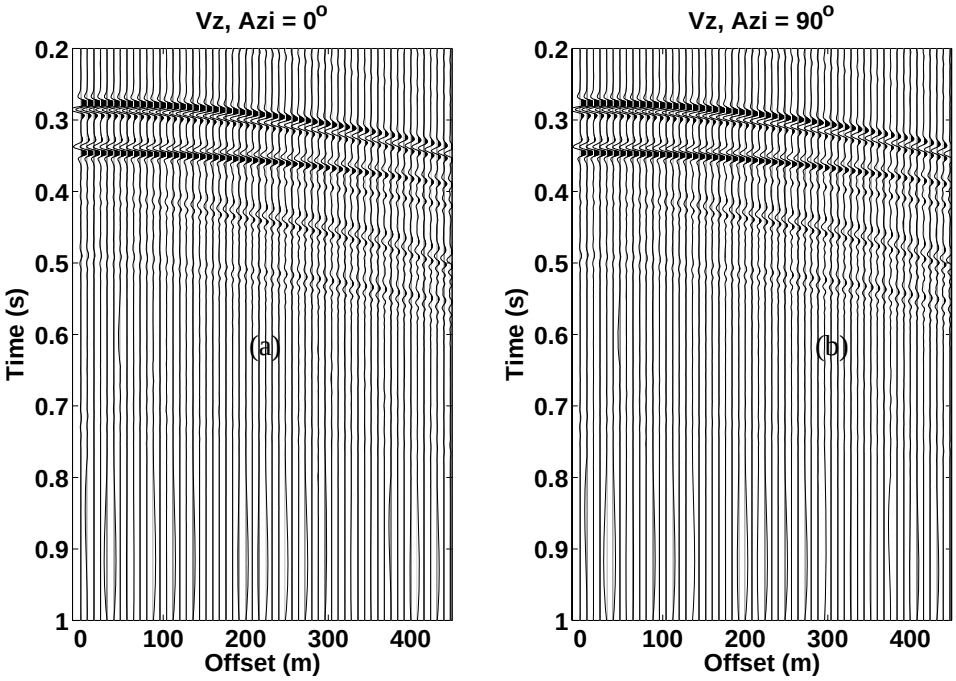

Figure 9: Shot gathers for the three layer base model.

further analysis reveals that most of this energy is composed of S-waves. To compare seismograms for different fractured reservoir models, all the amplitudes of the seismograms are amplified 15 times. Comparing the shot gather at zero azimuth relative to x coordinate axis in Figures 9a and 10a, we easily identify the reflected and converted modes at the top and bottom of the reservoir. At near offsets of Figure 10a for zero azimuth, we see backscattered waves with almost the same slowness arrive as late as 0.7 s. The early arrivals of the backscattered waves interfere the PP wave reflected from the reservoir bottom, so they arrive at the receivers as P wave. However, the moveout velocity is slower than that of the P wave and the wavefront is almost linear, which indicates the wavefront of the backscattered waves due to the set of vertical fractures is similar to a plane wave. At far offsets, we observe that the converted PS and PSP waves from the reservoir bottom show strong interference by the scattered waves, while the PS reflection from the reservoir top can still be seen clearly. We also see strong coherent forward scattered waves following the PS reflection from the bottom of the second layer. These events appear to have velocities slower than that of the shear waves and form two plane wave packs. The dominance of backward scattering at near offsets and forward scattering at far offsets indicates seismic waves transmitted to the fractured layer are mainly reflected by and transmitted through the fracture sets at near and far offsets, respectively. In the middle range of offsets, the back scattered and forward scattered waves interfere and cause some cancellation. With the increase of azimuth, the backward scattered waves seem to become somewhat stronger and the wavefronts become flatter; the forward scattered waves become weaker.

At the 90 degree azimuth, where the receiver line is parallel to the fracture strike, the scattered waves appear to form coherent wavefronts from 0.5 s and later, parallel to that of the PS wave reflected off the bottom of the reservoir layer. The scattered waves also interfere with the PS wave from reservoir top and

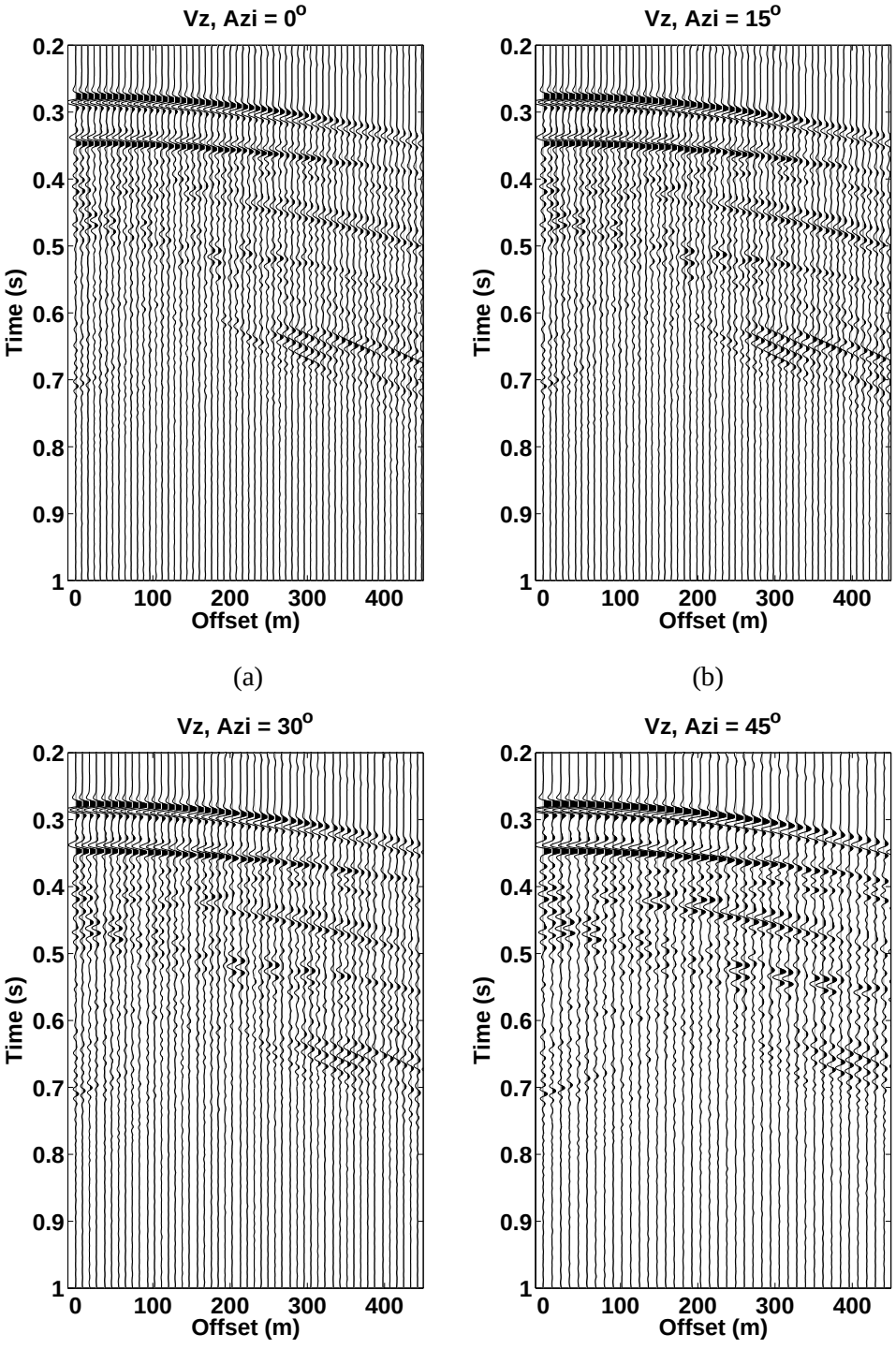

(a) (b)

(c) (d)

Figure 10: Shot gathers for a set of parallel fractures embedded in the middle layer

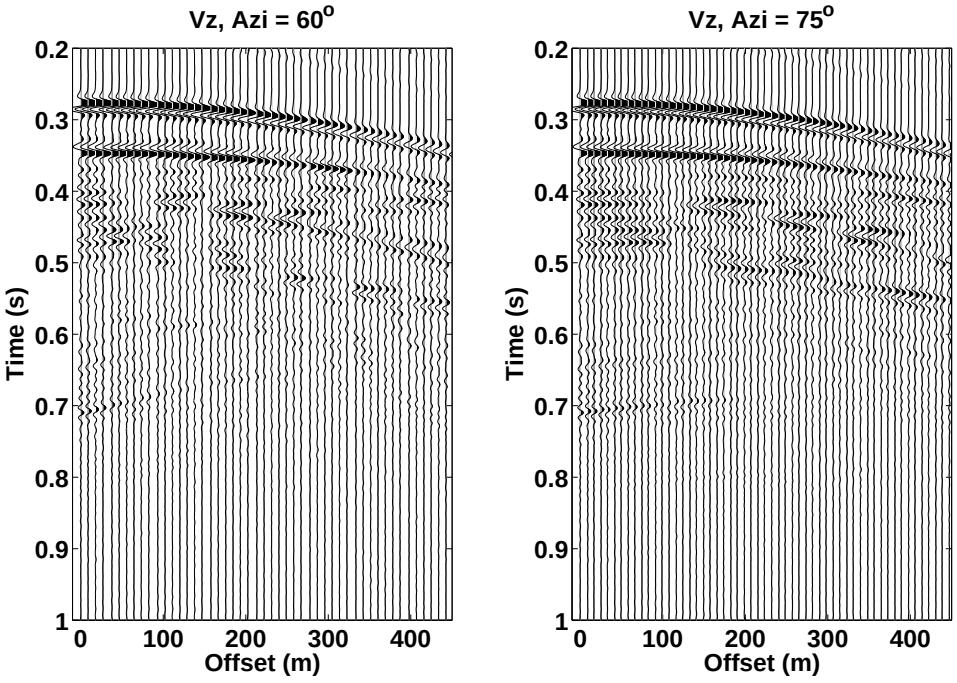

(a) (b)

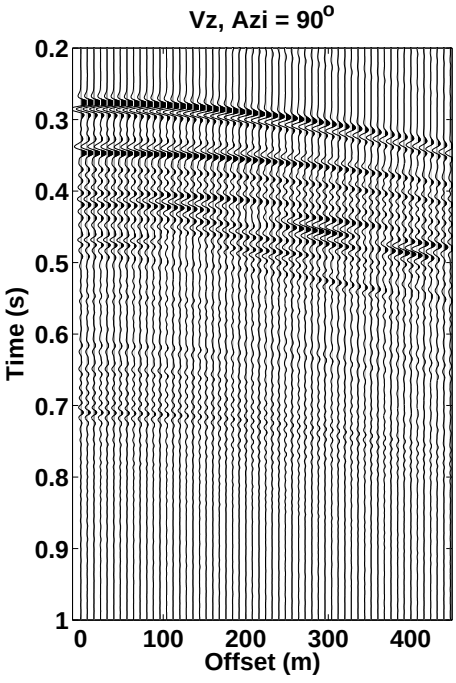

(c)

Figure 11: Shot gathers for a set of parallel fractures embedded in the middle layer

PSP from reservoir bottom and cause amplitude variations with offset.

In summary, we observe the following from the azimuthal shot gathers for the single set fracture model:

1. Seismic responses show azimuthal dependence;

2. Backscattering becomes stronger with increase of azimuth (less than 60 degrees). Forward scattering exists at all azimuths at far offsets. At 90° azimuth, the scattering forms coherent wavefronts, though tuning with offset appears.

3. The reflected PP from the top and bottom of the fractured layers are almost not affected and converted PS waves can be clearly seen up to 75 degree azimuth. At 90-degree azimuth, the scattering waves completely overwhelm the PS waves, but the scattered wavefronts seem to have the same moveout velocity as the converted PS wave from the bottom of the fractured layer.

Figure 12 and 13 show shot gathers for two sets of orthogonally intersecting fractures embedded in the middle layer. Because the model is completely symmetric relative to the 45-degree azimuth, and the two sets of fractures are of the same compliance, the gathers at 0 and 90 degrees are the same. They show the combination of characteristics of the scattering waves due to the single set of fractures at 0 and 90 degrees as shown in Figure 10a and 11c. In other words, we observe both back and forward scattering at near and far offsets, respectively imposed upon the coherent scattered waves, though the scattering seems stronger than that in the single fracture case. The reflected PP arrival from the bottom also shows strong interference by the scattered waves. At the 45-degree azimuth, the scattered waves become strong and appear at all offsets. Figure 14 shows the snapshots (a) in a horizontal plane crossing the fractured layer and (b) in a vertical plane including the source position parallel to the x axis. In the horizontal plane, the incident wave keeps the circular shape of its wavefront, but the wavefield within the fractured medium mirrors the fracture distribution. The snapshot in the vertical plane (Figure 14b) shows the incident wavefront is separated by the vertical fractures. The reflected P wave from the top of the reservoir is not affected, but the waves that follow it show considerable interference. At far offsets, the effects of the elastic property distribution on wave propagation are more complicated than those at the near offsets.

5.2 Orthogonally intersecting sets of different spacing

To study the sensitivity of the scattered wavefield to the spacing of the orthogonal fracture sets, we choose the spacing of the fracture set with orientation at 90 degree and 0 degree azimuths to be 30 m and 42 m, respectively. Figures 15 and 16 show the shot gathers. The gathers at 0 and 90 degree azimuths also show the combination of characteristics of the scattering waves due to the single set of fractures at 0 and 90 degrees as shown in Figure 10. However, the coherent scattering due to the fracture set of 42 m spacing is less pronounced than the 30 m one. The converted PS and PSP waves from the top and bottom of the fractured layer are still recognizable from the 0 azimuth shot gather. At the 90-degree azimuth, the reflected PP arrival from the bottom also shows strong interference by the scattered waves and the converted waves are difficult to identify. Therefore, the spacing of a fracture set significantly affects the scattering pattern.

5.3 Orthogonally intersecting sets of different compliances

If the two principal horizontal stresses are of different magnitudes, it will cause the fracture sets to have different compliances. To investigate the scattering of seismic waves due to two sets of intersecting fractures of different compliances, we choose the same 30 m spacing for the orthogonal sets of fractures, but the compliance of the set parallel to x axis is four times of that of the set normal to the x axis. The less

compliant fracture has the same compliance as those for the model with equal strength fracture sets. Figure 17 shows shot gathers at 0 and 90 degree azimuths. Comparing them with the gathers at the same azimuths in Figure 12a (the gathers at 0 and 90 degree azimuths are the same due to geometric symmetry of the model used for generating Figure 14), we see at 0 degree azimuth, parallel to the more compliant fracture set, the coherent scattered waves are much stronger than that from the more rigid fracture set whose orientation is at 90 degree azimuth. Strong forward and backward scattering appears at almost all offsets in the gather at 90 degree azimuth besides the coherent scattering due to fracture set oriented at 90 degree azimuth. The scattered waves due to the more compliant set also last much longer to around 0.9 s.

6 Case 2: Two 45-degree intersecting fracture sets

Figure 18 shows the model for non-orthogonally intersecting fracture sets, which make a 45-degree angle. As in Figure 8, the different colors in Figure 19 represent the background, the two sets of fractures and their intersections. The spacing of the set normal to the x axis is 30 m, and the spacing of the other set at 45-degree azimuth is 42 m. Both sets of fractures have the same compliance. The finite difference cells neighboring the intersections of the fractures can be assigned the same anisotropic properties computed using effective media theory, since the cell size is much smaller than the seismic wavelength. Here we choose 9 cells surrounding an intersection including the intersection itself. Average properties of the neighboring cells can also be considered when assigning properties to each cell. This will be a bit more complicated, but we do not expect it will make much difference since the size of the intersection area is about one order of magnitude smaller than the seismic wavelength.

The gathers in Figure 20 are best compared with those for the orthogonal intersecting fracture sets in Figures 12 and 13 and those for a single fracture set in Figures 10 and 11. At the 0-degree azimuth, the shot gather is similar to that for the single set of fractures. The 45 degree oriented fracture set apparently increases the forward scattering at far offsets. Otherwise, this gather does not show much sensitivity to the fracture set at the 45-degree azimuth. At the 90 degree azimuth, the gather shows significant forward scattering coming from the 45 degree oriented fracture and weak backward scattering. The coherent scattered waves are still clear around 0.4 – 0.5 s, but they show significant interference at later time from 0.6 and afterward. The shot gather at 45-degree azimuth shows coherent scattering mimicking those of 90-degree azimuth, since the receiver line is parallel to the orientation of one fracture set. Comparing to the gather at 90-degree azimuth, we see the scattering coming from the fracture set of shorter spacing is stronger and interferes with the coherent scattering.

Figure 21 shows the snapshots (a) in a horizontal plane crossing the fractured layer and (b) in a vertical plane including the source position parallel to the horizontal axis for the model including the two sets of non-orthogonally intersecting fractures. In the horizontal plane, the wavefront of the point source is still circular, but the wavefield within the fractured medium mirrors the fracture distribution, particularly at near offsets. The snapshot in the vertical plane Figure 21b shows the incident wavefront is divided by the vertical fractures in both azimuths. The reflected P wave from the top of the fractured layer is not affected. The waves that follow it show stronger interference than those in Figure 14 and the wavefield becomes more complex.

7 Conclusions

We describe a novel method for using a finite difference scheme to simulate wave propagation in media with intersecting fracture sets. We use effective media theory to compute the anisotropic elastic stiffness

for finite difference cells containing any segments of a fracture and assign the properties to those cells. Surrounding the intersections of the fracture sets, we use the long wavelength approximation and treat the cells as homogeneous to simplify the elastic stiffness calculation. Our implementation uses the rotated staggered grid and perfectly matched layer absorbing boundary condition to achieve good accuracy for scattered wave study.

We then use the finite difference program to model the wave propagation in layered formations with one set of parallel fractures, two sets of orthogonally intersecting fractures with the same spacing, different spacing, and different compliances, and two sets of non-orthogonally intersecting fractures. The reflected P waves from the top and bottom of the fractured layer are not significantly affected by the presence of the fracture sets. The converted PS and PSP waves from the bottom of the fractured layers show strong interference except at small azimuths. We observe coherent scattered waves in shot gathers parallel to the fracture orientation and significant backscattering at near offsets and forward scattering at far offsets. The scattering pattern varies azimuthally. When two sets of fractures are present, scattering becomes stronger and more complex scattered waves appear in the gathers. The shorter the spacing and the more compliant the fracture, the stronger the scattering. When the fracture sets are not orthogonal to each other, the gathers still show coherent scattering in the fracture orientations. By capturing the azimuthal characteristics of the scattered waves, one can analyze fracture orientations, spacing, and relative compliance of intersecting fracture sets. Detailed analysis of reflected and converted wave data obtained by using the proposed modeling method, may provide insights on the applicability of effective media theory in fracture characterization. The modeling method also provides a new, widely applicable tool for understanding seismic data from fractured reservoirs.

8 Acknowledgements

This work is funded by the ERL Founding Members Consortium. Additional support comes from Shell GameChanger.

References

Auld, B. A. (1990). *Acoustic fields and waves in solids, Volume I.* Robert E. Krieger Publishing Co.

Bakulin, A., Grechka, V., and Tsvankin, I. (2000a). Estimation of fracture parameters from reflection seismic data, Part I : HTI model due to a single fracture set. *Geophysics*, 65:1788–1802.

Bakulin, A., Grechka, V., and Tsvankin, I. (2000b). Estimation of fracture parameters from reflection seismic data, Part II : Fractured models with orthorhombic symmetry. *Geophysics*, 65:1803–1817.

Bakulin, A., Grechka, V., and Tsvankin, I. (2000c). Estimation of fracture parameters from reflection seismic data, Part III : Fractured models with monoclinc symmetry. *Geophysics*, 65:1818–1830.

Coates, R. T. and Schoenberg, M. (1995). Finite-difference modeling of fdaults and fractures. *Geophysics*, 60:1514–1526.

Grechka, V. and Kachanov, M. (2005). Multiple fractures in rocks: Effectiuve orthotropy and seismic characterization. In *Exp. Abstr., 75th Ann. Internat. Mtg.*, pages 158–161. Soc. of Expl. Geoph.

Hudson, J. A. (1986). Overall properties of a material with inclusions or cavities. *Geophys. J. Int.*, 117:555–561.

Liu, E., Hudson, J. A., and Pointer, T. (2000). Equivalent medium representation of fractured rock. *J. Geophys. Res.*, (105):2981–3000.

Lynn, H. B. (2004). The winds of change. *The Leading Edge*, 21(11):1156–1268.

Marcinkovich, C. and Olsen, K. (2003). On the implementation of perfectly matched layers in a three-dimensional fourth-order velocity-stress finite-difference scheme. *J. Geophys. Res. B*, 108(5):18–1–18–16.

Nelson, R. A. (1985). *Geologic analysis of naturally fractured reservoirs*. Gulf Publishing, Houston, TX.

Nichols, D., Muir, F., and Schoenberg, M. (1989). Elastic properties of rocks with multiple sets of fractures. In *Exp. Abstr., 59th Ann. Internat. Mtg.*, pages 471–474. Soc. of Expl. Geoph.

Nihei, K. T., Nakagawa, S., and Meyer, L. R. (2002). Finite-difference modeling of seismic wave interactions with discrete, finite-length fractures. In *Exp. Abstr., 72th Ann. Internat. Mtg.*, pages 1784–1751. Soc. of Expl. Geoph.

Reiss, L. (1980). *The reservoir engineering aspects of fractured formations*. Editions Technip, Paris.

Saenger, E. H., Gold, N., and Shapiro, S. A. (2000). Modeling the propagation of elastic waves using a modified finite-difference grid. *Wave Motion*, 31:77 – 92.

Sayers, C. M. (1998). Misalignment of the orientation of fractures and the orincipal axes for P and S waves in rocks containing multiple non-orthogonal fracture sets. *Geophys. J. Int.*, 133:459–466.

Schoenberg, M., Dean, S., and Sayers, C. M. (1999). Azimuth-dependent tuning of seimsic wave reflected from fractured reservoirs. *Geophysics*, pages 1160 – 1171.

Schoenberg, M. and Helbig, K. (1997). Orthorhombic media: modeling elastic wave behavior in a vertically fractured Earth. *Geophysics*, 62:1954 – 1974.

Schoenberg, M. and Muir, F. (1989). A calculus for finely layered anisoitropic media. *Geophysics*, 54:581 – 589.

Schoenberg, M. and Sayers, C. M. (1995). Seismic anisotriopy of fractured rock. *Geophysics*, 60:204 – 211.

Shen, F., Zhu, X., and Toksöz, M. N. (2002). Effects of fractures on NMO velocities and P-wave azimuthal AVO response. *Geophysics*, 67:711 – 726.

Vetri, L., Loinger, E., Gaiser, J., Grandi, A., and Lynn, H. (2003). 3D/4C Emilio: Azimuth processing and anisotropy analysis in a fractured carbonate reservoir. *The Leading Edge*, 22:675 – 679.

Virieux, J. (1986). Velocity-stress finite-differene method. *Geophysics*, 51:889 – 901.

Vlastos, S., liu, E., Main, I. G., and Li, X.-Y. (2003). Numerical simulation of wave propagation in media with discrete distributoins of fracturesl effects of fracture sizes and spatial distributions. *Geophys. J. Int.*, 152:649–668.

Willis, M. E., Burns, D. R., Rao, R., Minsley, B., Toksöz, M. N., and Vetri, L. (2006). Spatial orientation and disrtibution of reservoir fractures from scattered seismic energy. *Geophysics, in press*.

Willis, M. E., Rao, D. R. B. R., Minsley, B., Toksöz, M. N., and Vetri, L. (2004a). Spatial orientation and distribution of reservoir fractures from scattered seismic energy. In *Ext. Abstr. 74th Ann. Intern. Mtg.* Soc. Expl. Geophys.

Willis, M. E., Rao, R., Burns, D. R., Byun, J., and Vetri, L. (2004b). Reservoir fracture orientation and density from reflected and scattered seismic energy. In *Ext. Abstr., 66th Mtg.* Europ. Assn. Geophys. Eng.

Winterstein, D. F. (1990). Velocity anisotropy terminology for geophysicists. *Geophysics*, 55:1070–1088.

Zhang, Y., Chi., S., Willis, M. E., Burns, D. R., and Toksöz, M. N. (2005). Comparison of discrete fracture and effective media representation of fractures on azumuthal avo. In *Exp. Abstr., 75th Ann. Internat. Mtg.* Soc. of Expl. Geoph.

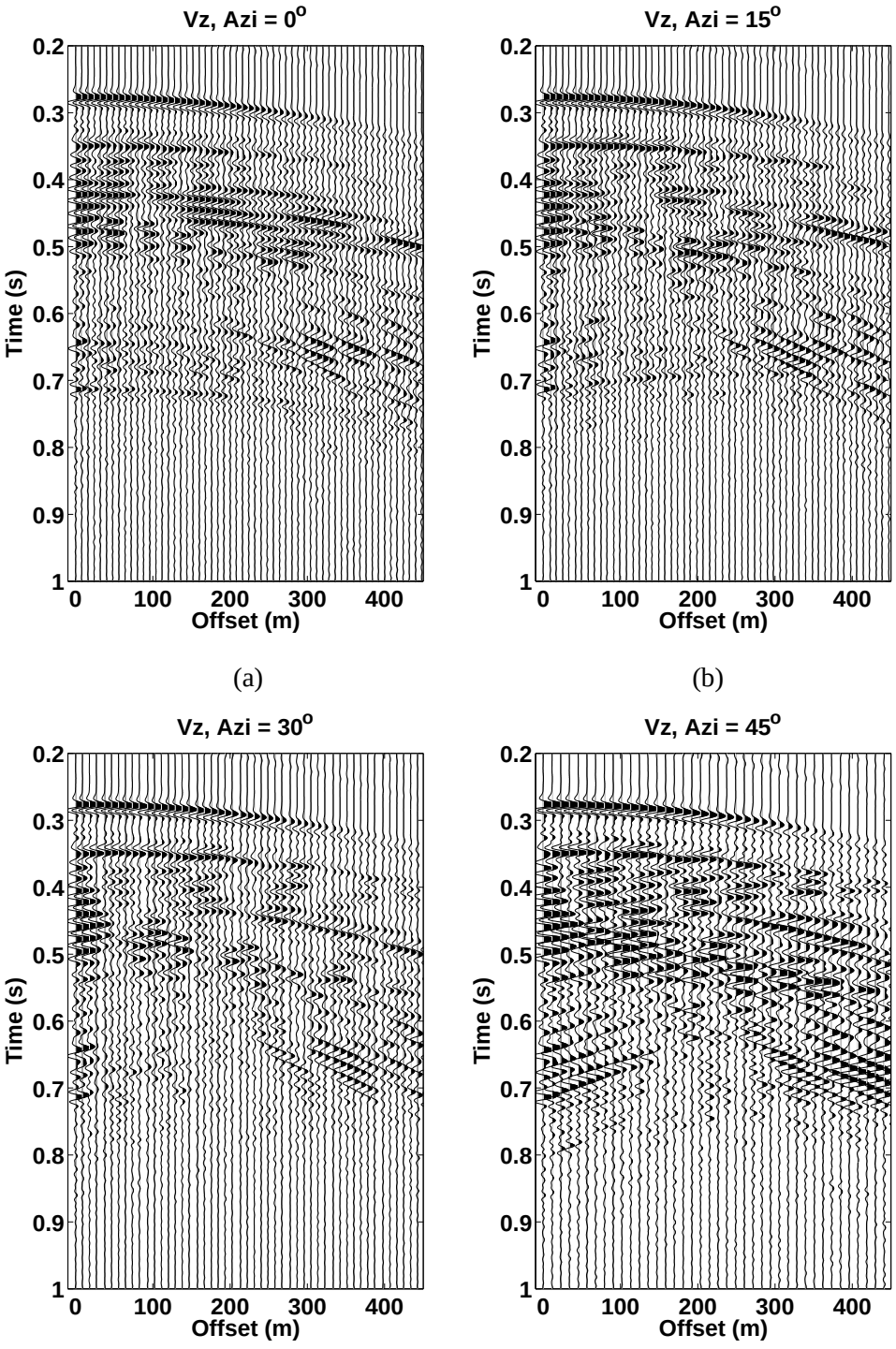

(a) (b)

(c) (d)

Figure 12: Shot gathers for two sets of orthogonally intersecting fractures embedded in the middle layer. The spacing of each set of fractures is 30 m.

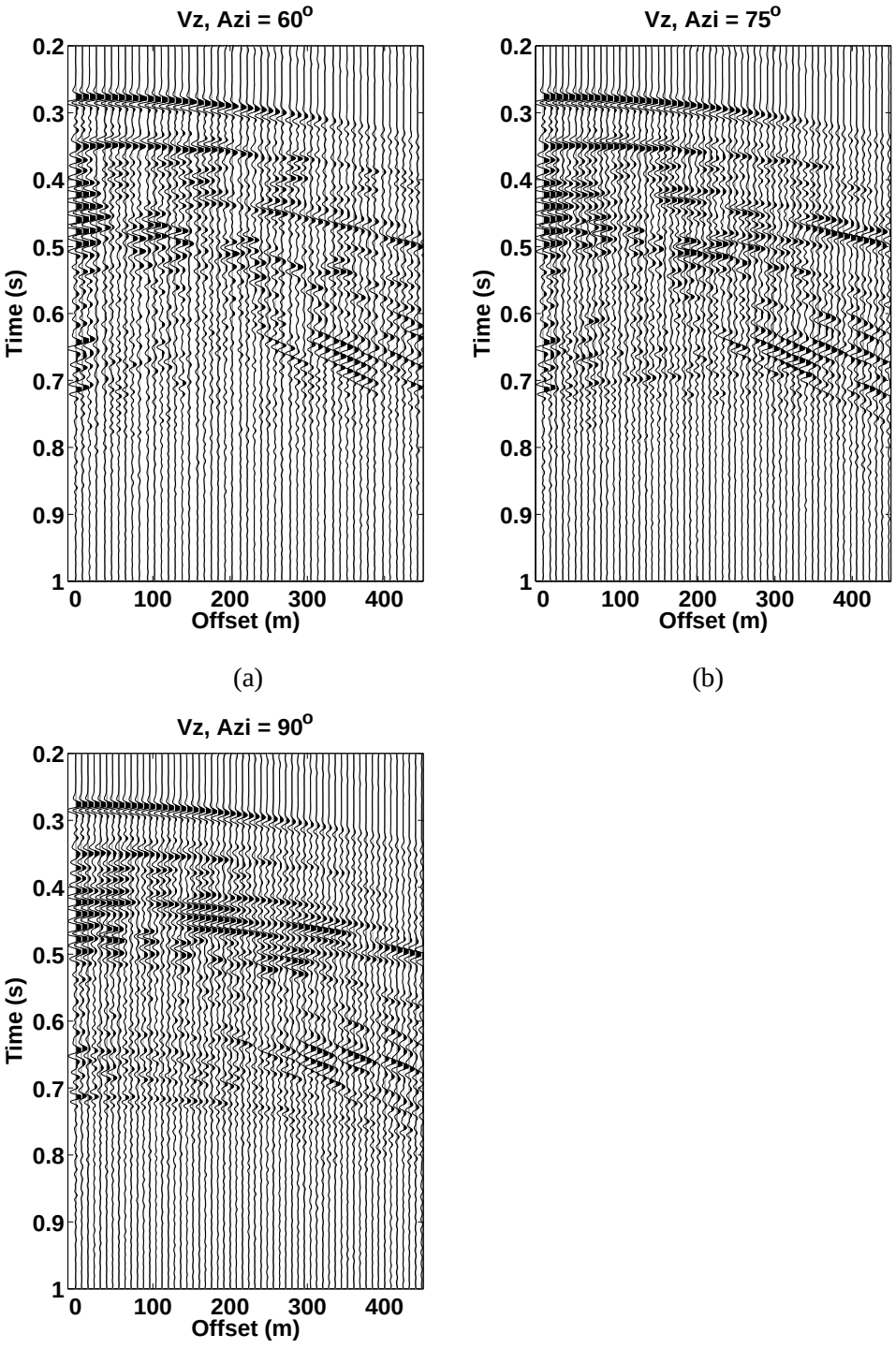

Figure 13: Shot gathers for two sets of orthogonally intersecting fractures embedded in the middle layer. The spacing of each set of fractures is 30 m.

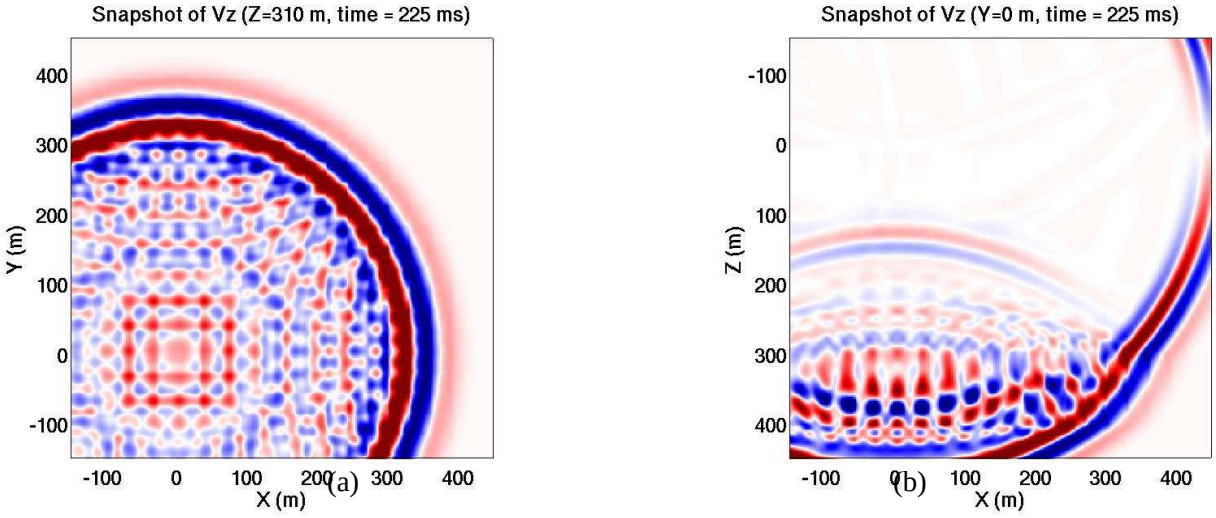

Figure 14: Snapshots of the wavefield in the fractured reservoir (a) in a horizontal plane at z=310 m; (b) in a vertical plane at y=0 m.

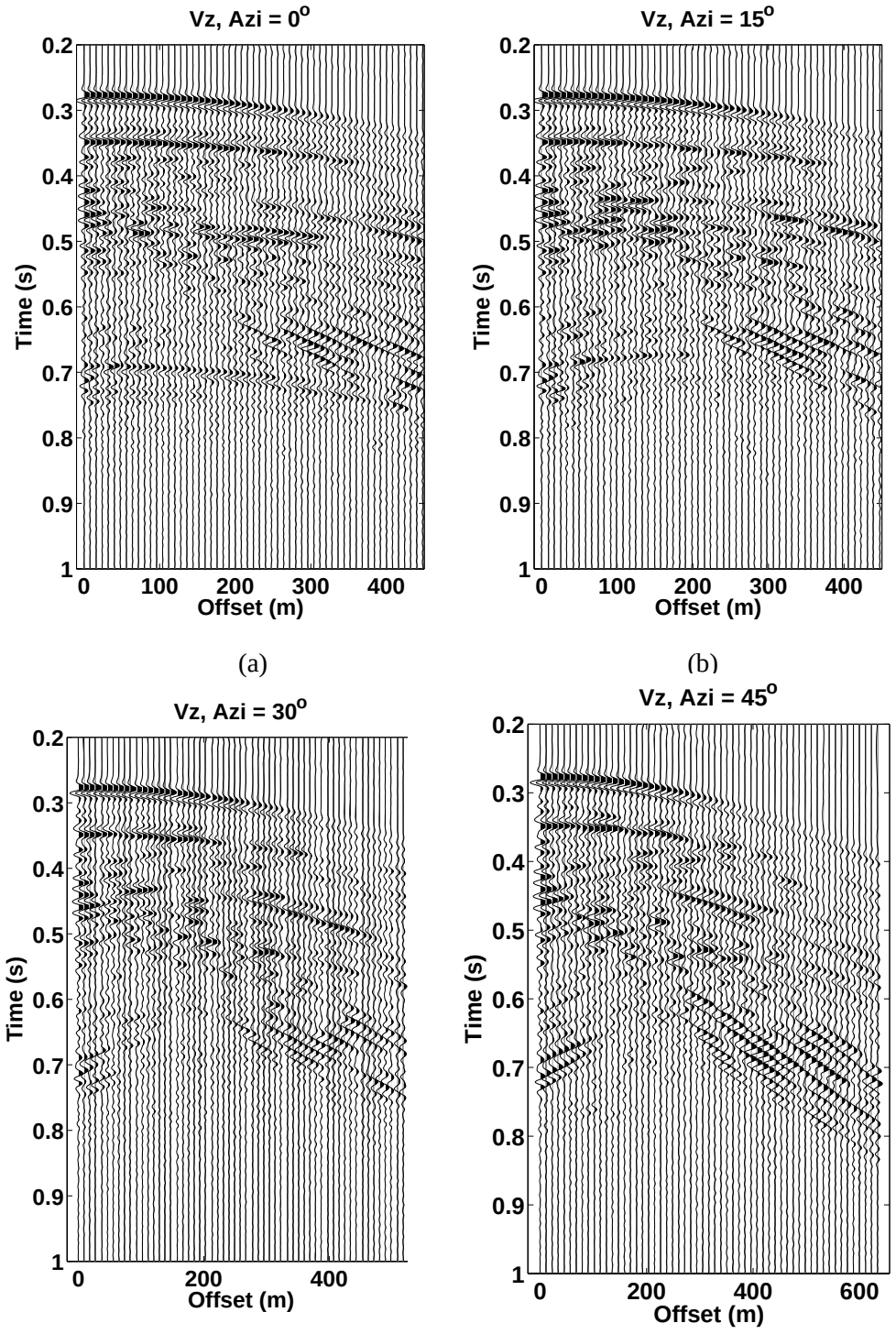

(a) (b)

(c) (d)

Figure 15: Shot gathers for two sets of orthogonally intersecting fractures embedded in the middle layer. The spacing of each set of fractures is 30 m and 42 m, respectively.

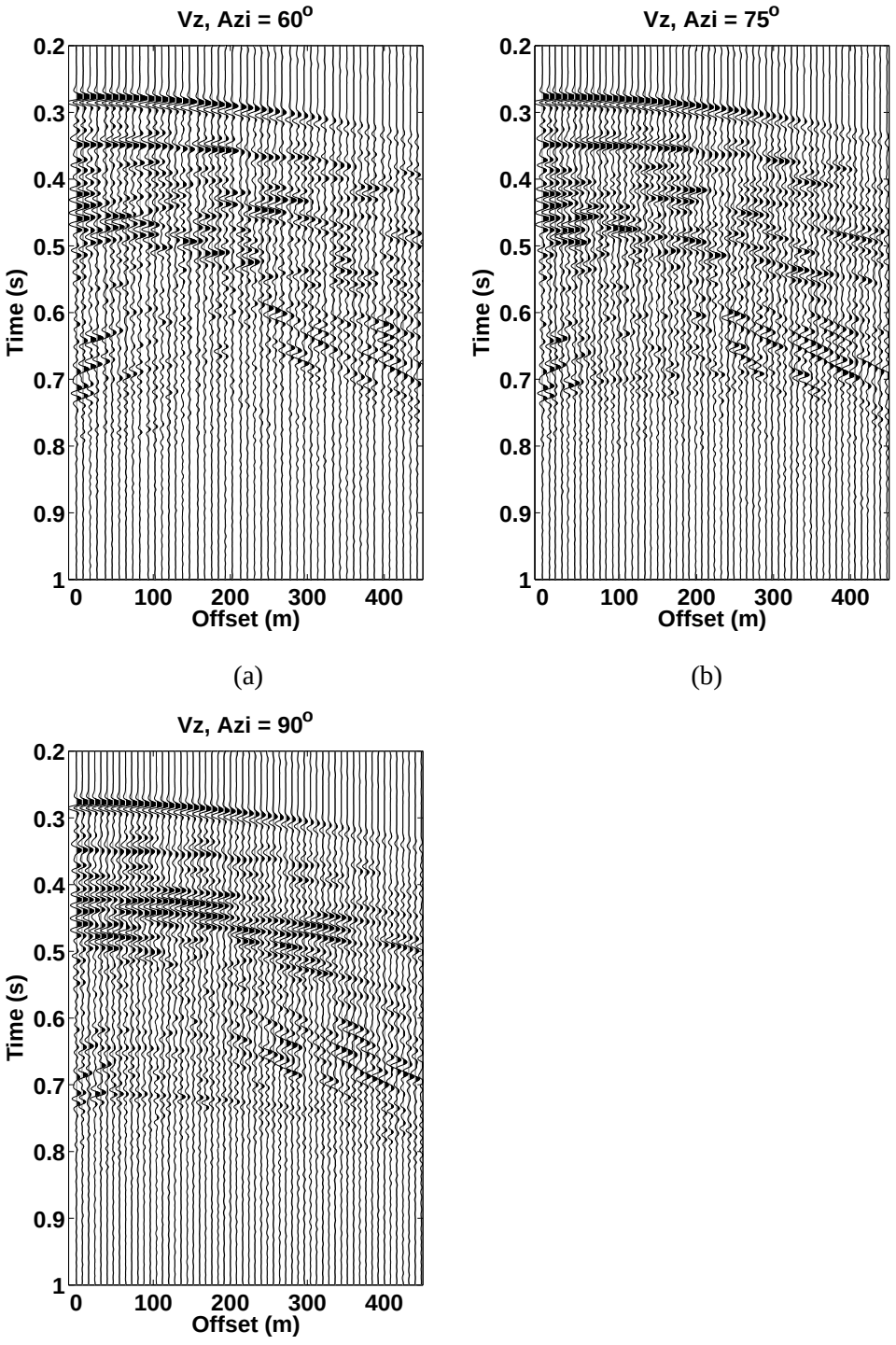

Figure 16: Shot gathers for two sets of orthogonally intersecting fractures embedded in the middle layer. The spacing of each set of fractures is 30 m and 42 m, respectively.

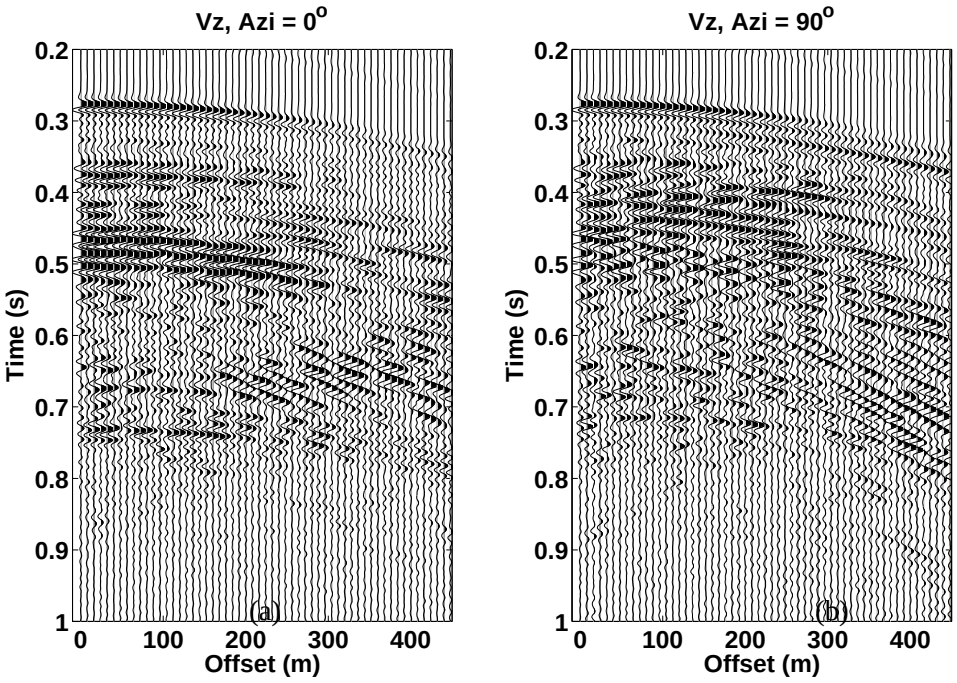

Figure 17: Shot gathers for two sets of orthogonally intersecting fractures embedded in the middle layer. The spacing of each set of fractures both is 30 m. The fracture set oriented at the 0 degree azimuth is four times as compliant as the one oriented at the 90-degree azimuth.

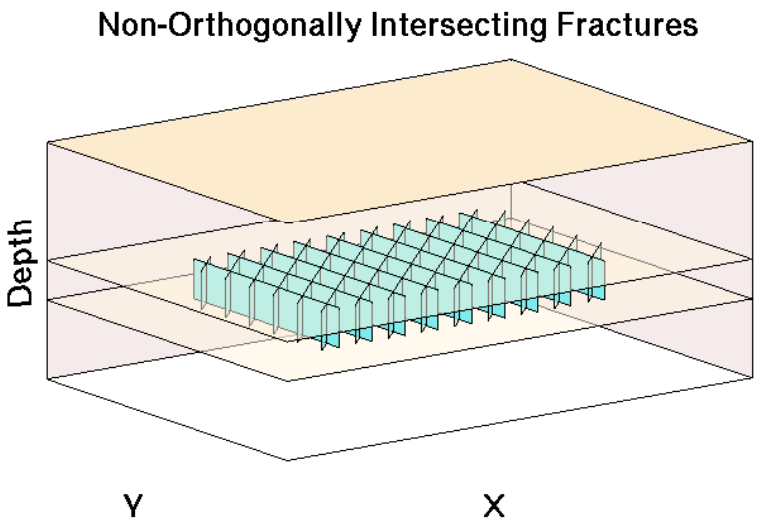

Figure 18: A 3D schematic of the reservoir model with two sets of intersecting fractures with an angle of 45 degrees.

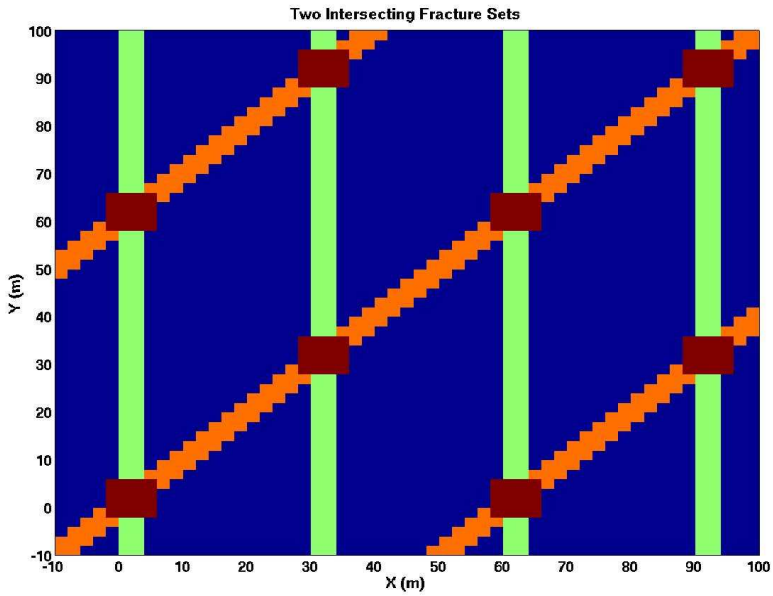

Figure 19: Elastic property distribution of two sets of 45 degrees intersecting fractures as indicated by different colors.

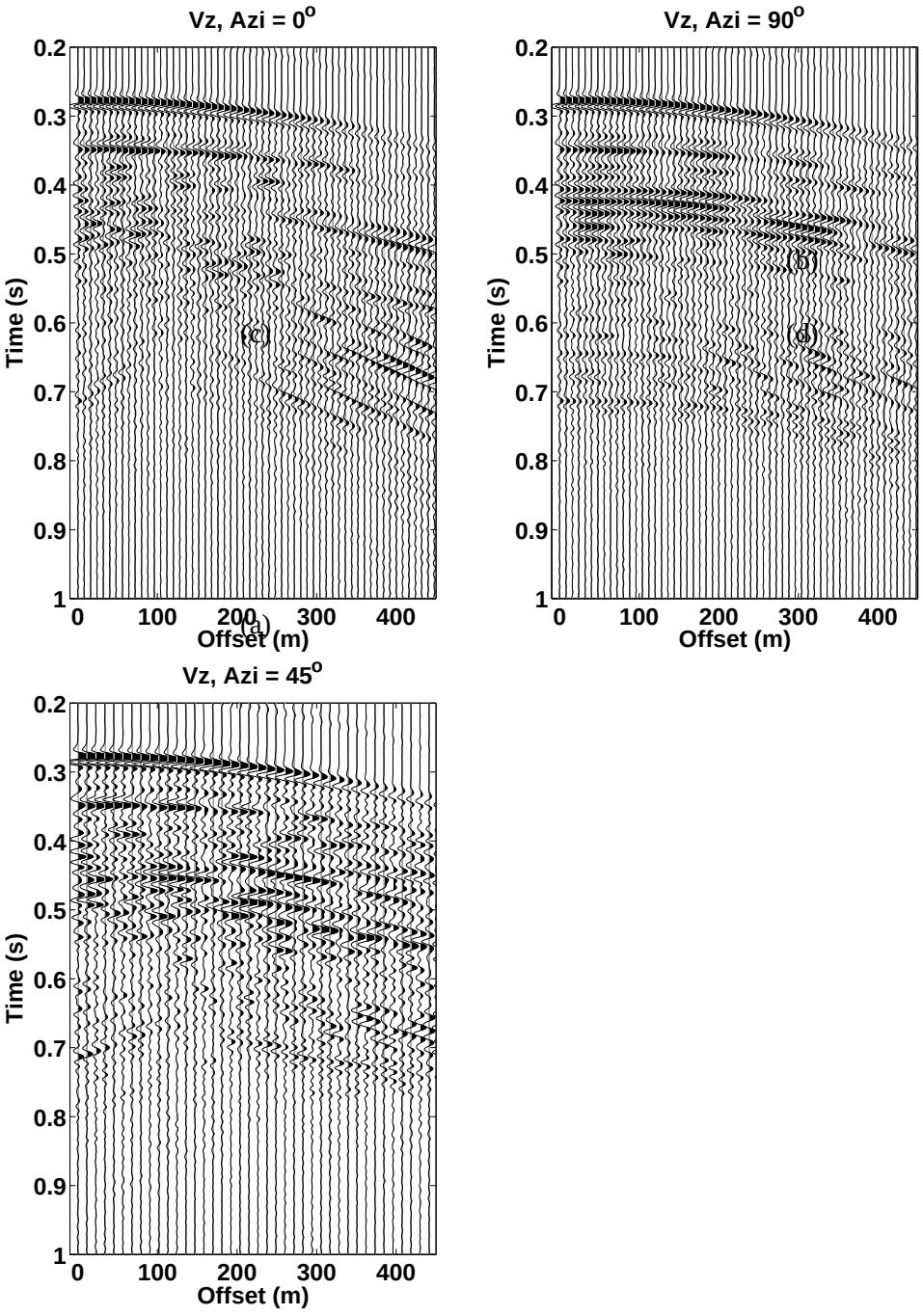

Figure 20: Shot gathers of vertical velocity measured on the surface of a fractured reservoir at 0, 90 and 45-degree azimuths.

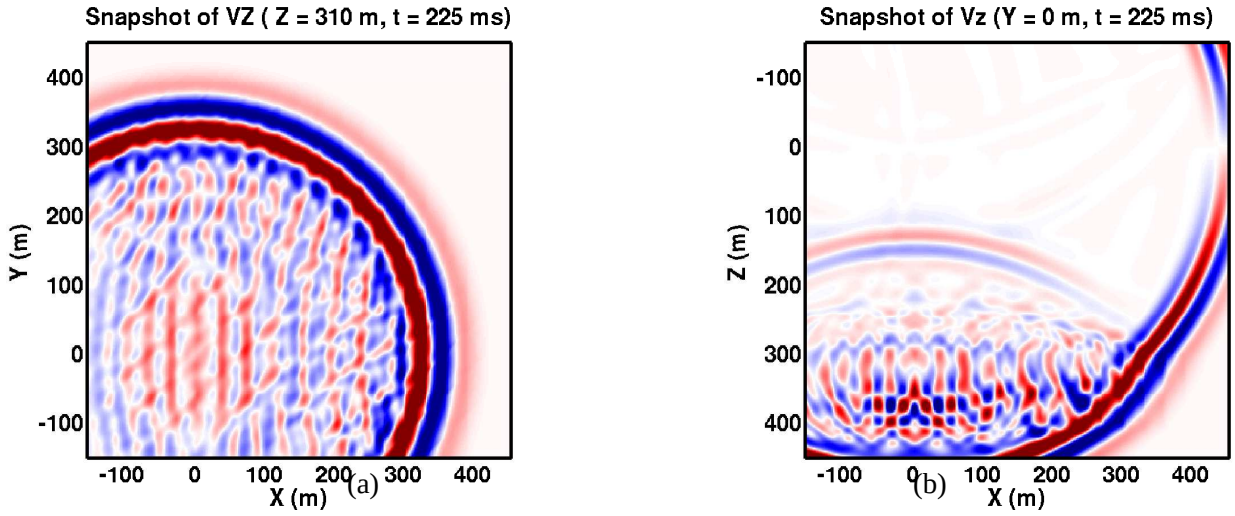

Figure 21: Snapshots of the wavefield in the fractured reservoir (a) in a horizontal plane at z=310 m; (b) in a vertical plane at y=0 m.